ELSEVIER

Biophysical Chemistry 122 (2006) 143–155

Biophysical Chemistry

http://www.elsevier.com/locate/biophyschem

Electron-transfer mechanism of the triplet state quenching of aluminium tetrasulfonated phthalocyanine by cytochrome *c*

César A.T. Laia [a,*], Sílvia M.B. Costa [a,1], L.F. Vieira Ferreira [b]

[a] *Centro de Química-Estrutural, Complexo 1, Instituto Superior Técnico, 1049-001 Lisboa, Portugal*
[b] *Centro de Química-Física Molecular, Complexo 1, Instituto Superior Técnico, 1049-001 Lisboa, Portugal*

Received 19 December 2005; received in revised form 9 March 2006; accepted 9 March 2006
Available online 12 March 2006

Abstract

The mechanism of electron-transfer from aluminium tetrasulfonated phthalocyanine triplet state to cytochrome *c* was investigated in this work. This reaction successfully quenches the dye triplet state due to the formation of complexes between the solute and the protein at the active site. The electron-transfer rate constant is around 3×10^7 s^{-1}, and is in accordance with previous results for the singlet excited state quenching [C.A.T. Laia, S.M.B. Costa, D. Phillips, A. Beeby. Electron-transfer kinetics in sulfonated aluminum phthalocyanines/cytochrome c complexes, J. Phys. Chem. B 108 (2004) 7506–7514.] in the framework of the Marcus theory, with a reorganization energy equal to 0.94 eV. The complex formation is diffusion controlled, but heterogeneities of the protein surface charge distribution lead to quenching rate constants smaller than predicted on a hard-spheres model with electrostatic interactions. Also the binding equilibrium constant is strongly affected by this phenomenon. Ionic strength plays an important role on the complex formation, but its effect on the unimolecular electron-transfer rate constant is negligible within experimental error.

Keywords: Cytochrome *c*; Phthalocyanine; Laser flash photolysis; Photoinduced electron-transfer; Triplet; Excited state

1. Introduction

The mechanisms underlying the interactions between proteins and substrates are an important step in order to understand biochemical reactions. Such interactions reveal a strong affinity and specificity, showing the importance of the solute architecture to induce the docking at the protein active site. This specific binding can be disrupted if other molecules appear with an even stronger affinity towards the active site. The design of highly functionalised molecules that can disrupt protein–ligand interactions has lead to a new insight towards the details of protein binding sites and to the inhibition of protein activity [1]. Much work has been carried out with cytochrome *c* (Cyt *c*), a protein that exists inside the mitochondria and plays major roles in respiration and apoptosis [2,3]. Cyt *c* is well known as an electron carrier in the mitochondria, from cytochrome *b5* to cytochrome *c* oxidase, undergoing electron-transfer reactions both as acceptor and donor depending on its oxidative state. Its structure is well known [4] and the active site that enables the interaction of Cyt *c* with proteins like Cytochrome *c* Oxidase and Caspases (in apoptosis) has a positively charged surface constituted by lysine residues [1,4–6]. Negatively charged synthetic solutes could therefore interact strongly with the Cyt *c* active site due to the strong electrostatic interactions that take place even in aqueous solutions [1,7–29]. The binding to synthetic solutes can even disrupt interactions with cytochrome *c* oxidase, modulate the protein function and induce the protein unfolding [1,15–26]. Such specific interaction is driven by electrostatic and hydrophobic interactions as well, and it leads to an efficient electron-transfer from the ligand to the Cyt *c* [8–10,12–14,27–29].

Recently it was shown that porphyrin derivatives could reduce the temperature at which the Cyt *c* unfolding occurs by

* Corresponding author. Present address: Departamento de Química, CQFB-REQUIMTE, Laboratorio de Fotoquimica e Quimica Supramolecular, Faculdade de Ciencias e Tecnologia, Universidade Nova de Lisboa, Quinta da Torre, 2829-516 Monte de Caparica, Portugal. Tel.: +351 218419274; fax: +351 218464455.
E-mail address: cesar.laia@dq.fct.unl.pt (C.A.T. Laia).
[1] Tel.: +351 218419274; fax: +351 218464455.

0301-4622/$ - see front matter © 2006 Published by Elsevier B.V.
doi:10.1016/j.bpc.2006.03.003

as much as 20 °C [18,19,21]. Other negatively charged solutes like calixarenes, [25] SDS micelles [30] and sulfonated polystyrene polymers [26] induce major changes on the conformation of Cyt *c*, although they may not reflect a complete loss of ability to undergo electron-transfer reactions [25]. It is also known that, in the mitochondria, Cyt *c* binds to the membrane where the electron-transfer reactions occur, [31] but membranes can induce conformational changes as well [32]. Cyt *c* electron-transfer properties depend a lot on the native Met80–Fe(III) axial bond, [33] which can be reconstituted even if the protein is separated into two peptide fragments [34]. Thus a direct link between conformational change and loss of activity in these processes is not straightforward, and the way these aspects may interplay in the electron-transfer process is not completely known.

The dye tetrasulfonated aluminium phthalocyanine ($AlPcS_4$) is a synthetic organic molecule with 4-charges, well known due to its photodynamic therapy applications in cancer treatment [35]. Due to its suitable chemical structure $AlPcS_4$ indeed forms complexes with Cyt *c*, leading to a strong quenching of the singlet excited state via an electron-transfer reaction [28,29]. The binding constant in water is quite high (3×10^5 M^{-1}), and the fluorescent complexes could be studied by time-resolved fluorescence kinetics. The electron-transfer reaction between the $AlPcS_4$ singlet excited state and Cyt *c* is fast, with the rate constant reaching as much as 10^9 s^{-1}. This effect is not only observed in aqueous solutions, [28] but also on micelles and reversed micelles with non-ionic surfactants, in environments which are quite apolar [29]. In ionic micelles such as those from SDS this process is lost because the electrostatic interactions that lead to the formation of the complex are disrupted, an effect also observed when the ionic strength is increased.

In this work we explore the interactions between the $AlPcS_4$ triplet state and Cyt *c* using Laser Flash Photolysis techniques. The ionic strength effect was studied with greater detail, because electron-transfer from the $AlPcS_4$ triplet state to Cyt *c* is much slower, allowing a study of the bimolecular reaction of the isolated species (on the singlet excited state quenching, only the unimolecular reaction on the complex was studied). The conditions where $AlPcS_4$ can change the conformational state of Cyt *c* were studied through Circular Dichroism spectroscopy. This technique is able to probe the chirality of the Cyt *c heme* group [36] and the protein secondary structure. It is observed that for $AlPcS_4$ concentrations around 10^{-5} M, Cyt *c* structure is changed but a complete unfolding does not occur.

2. Experimental

$AlPcS_4$ was purchased from Porphyrin Products (99% purity) and used as received. The phthalocyanine reagent is a mixture of 3 regioisomers. Previous work with disulfonated phthalocyanines showed that the photophysical properties remain unchanged in all isomers [35]. Cyt *c* was purchased from Aldrich (97% purity) and used without further purification as well. Bidistilled water was used in all experiments.

Absorption spectra were recorded at room temperature with a JASCO V-560 UV/VIS absorption spectrophotometer.

The triplet decay kinetics was recorded using a laser flash photolysis equipment using the second harmonic (532 nm, 65 mJ, 8 ns) of a Nd-YAG laser (Spectra-Physics, System Quanta-Ray GCR-3) as an excitation source to pump a rhodamine 6G dye laser (Spectra-Physics, System Quanta-Ray PDL-2) tuned at 570 nm with laser pulses of ~6 ns. The kinetic spectrophotometer (10 ns resolution) included an averaging system consisting of a Tektronix 2430A digital oscilloscope coupled with a personal computer (IBM compatible) [37]. Kinetic curves were averaged over at least 16 laser pulses. The rate constants were obtained by global analysis of the decays at several wavelengths with first order (mono-exponential) kinetics.

Transient-Absorption Spectra were obtained in another laser flash photolysis equipment, with the third or fourth harmonics of a Nd:YAG laser (355 and 266 nm, ca. 6 ns FWHM, 10–30 mJ $pulse^{-1}$) from B. M. Industries (Thomson-CSF Saga 12-10), in the transmission mode. The light was collected by a collimating beam probe coupled to an optical fibre (fused silica) and detected by a gated intensified charge-coupled device (Andor ICCD detector, based on the Hamamatsu S5769-0907). The ICCD was coupled to a fixed imaging compact spectrograph (Oriel FICS 77441). The system can be used either by capturing all the light emitted by the sample or in a time-resolved mode by using a delay box (Stanford Research Systems D6535). The ICCD has high speed gating electronics (2.2 ns) and intensifier and covers the 200–900 nm wavelength range. Time-resolved absorption and emission spectra are available in the nanosecond to second time range [38].

CD spectra were obtained with a Jasco spectropolarimeter J-720 (Hachioji City, Tokyo) [39]. The protein spectra were measured using 10 mm (for the Soret band) and 2 mm (for far UV measurements) quartz cells. The CD signal (in mdeg) was converted to molar ellipticity $[\theta]$ (deg cm^2 $dmol^{-1}$), defined as $[\theta]=\theta_{obs}(10\cdot c\cdot l)^{-1}$ where θ_{obs} is the experimental ellipticity, c the protein concentration (mol dm^{-3}) and l the cell path length (cm). The protein concentrations ranged between 5×10^{-6} and 1×10^{-5} M, depending on the experiment.

3. Results and data analysis

3.1. Circular dichroism spectra

The Cyt *c* structural changes can be probed using the Circular Dichroism (C.D.) spectroscopy. This technique allows the study of the *heme* group and of the secondary protein structure (namely the presence of α helixes and β sheets) by selecting suitable wavelength ranges [32,36,39–42]. The Soret band can be studied in detail in order to check (among other things) if there are axial bonds between the iron and another amino acid [40]. In the ultraviolet region the secondary structure is highlighted, disappearing when complete unfolding occurs. The unfolding can be usually induced by temperature increase and/or the addition of guanidinium chloride [43]. The presence of certain additives like synthetic receptors, micelles or polymers induces changes in these structures, which show that the presence of solutes has indeed a strong impact on the protein structure [18,19,21,26,30].

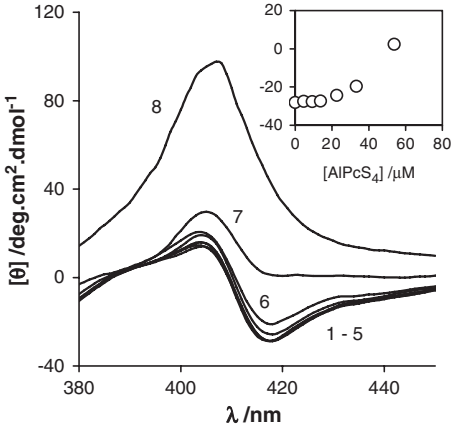

Fig. 1. Cyt *c* CD spectra for different [$AlPcS_4$] in aqueous solution without salt ([$AlPcS_4$]=0 μM (1), 4.5 μM (2), 9.2 μM (3), 13 μM (4), 23 μM (5), 33 μM (6) and 53 μM (7)). Curve 8 was made with guanidinium chloride (7 M) and corresponds to denatured Cyt *c*. Insert shows dependence of [θ] vs. [$AlPcS_4$] for λ=417 nm. [Cyt *c*]=10 μM.

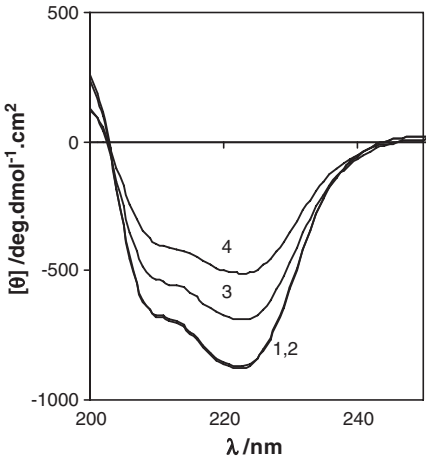

Fig. 2. Far-UV CD spectroscopy of Cyt *c* in aqueous solution without salt ([$AlPcS_4$]=0 μM (1), 10 μM (2), 25 μM (3) and 40 μM (4)).

$AlPcS_4$ does not show any optical activity within the spectral range 200 to 700 nm. The absorption spectrum of this molecule is characterized by a strong absorption at around 680 nm (the Q band) and 350 nm (the Soret band). But even in the presence of Cyt *c* no optical activity is observed at 680 nm, showing that although the active center has chirality, the protein does not have any effect on the molecular electronic spectra of the complexed dye. The Cyt *c* solutions without $AlPcS_4$ show the typical *heme* band in the region between 380 and 450 nm (Fig. 1). The CD spectra present two peaks, one negative and another positive, which have been assigned on account of the axial bond between Fe^{3+} and the histidine residue. By addition of $AlPcS_4$, at first no changes are found. At high concentrations, however, the negative feature disappears gradually and for the higher [$AlPcS_4$] the spectra are positive. It approaches a shape close to that found in unfolded Cyt *c*, but nevertheless such limit is far from being reached. It is possible that for even higher dye concentrations a complete Cyt *c* unfolded state is reached, because a plateau was not observed. However higher [$AlPcS_4$] means more absorption, which would lead to a saturation of the signal (for concentrations above 50 μM, Abs>5 for a cell with 1 cm thickness).

The evolution of the CD signal at 416 nm with [$AlPcS_4$] shows that for [$AlPcS_4$]<20 μM with [Cyt *c*]=10 μM no significant changes are observed, meaning that Cyt *c* is not affected by the presence of the additive. At first sight, it seems from Fig. 1 that at least a $(AlPcS_4)_2$Cyt *c* complex is required to unfold the protein. Inspecting the ultraviolet region (Fig. 2), the presence of α helixes is observed until [$AlPcS_4$]<20 μM. For higher concentrations the secondary structure disappears gradually, as it was observed in the Soret region, however the shape of the spectra remains the same. Therefore $AlPcS_4$ induces the unfolding of the α helixes, but a complete unfolded state is not reached. The link between the α helixes unfolding and the break of the *heme*-histidine axial bond is evident, showing that for [$AlPcS_4$]>20 μM large changes of the cytochrome *c* structure are induced.

The changes that Cyt *c* undergoes are slow, taking more than one hour to attain the final stable conformation (Fig. 3). A plateau is reached which depends on the composition, meaning that a complete conversion from the native species toward other states is not obtained and a dynamic equilibrium is reached. The kinetics exhibits single-exponential for low $AlPcS_4$ concentration, but at high concentrations the kinetics is clearly biexponential, although the timescale of the conformational change remains the same.

Finally for our purposes (to study the interactions between the $AlPcS_4$ triplet excited state with the protein, [$AlPcS_4$]= 10 μM) it is safe to say that Cyt *c* retains its structure. Hence their redox properties are unchanged and electron-transfer reactions can occur.

3.2. Triplet decays

Laser flash photolysis decays showed single-exponential kinetics at all [Cyt *c*] used (see Fig. 4) for [$AlPcS_4$]=10 μM. A wide range of absorption wavelengths from 350 to 700 nm was studied, but the decays at all wavelengths could be fitted globally with single-exponential kinetics. The transient

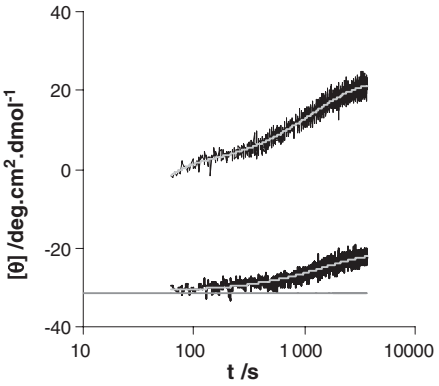

Fig. 3. Kinetics of the Cyt *c* unfolding with [Cyt *c*]=5 μM and [$AlPcS_4$]=20 μM (lower curve) and 40 μM (upper curve). Fits with exponential functions are also depicted. λ=416 nm.

absorption spectra had the same shape with or without Cyt *c*, and no indication of reduced Cyt *c* or oxidised $AlPcS_4$ was obtained within these experiments. The same applies to the situation in which phosphate buffer is added; the kinetics continues to be single-exponential within the range of concentrations explored on the present study. However, the effect of adding Cyt *c* is much smaller and both the triplet lifetime and triplet quantum yield are less affected in phosphate buffer solutions.

The triplet quantum yields ϕ_T were obtained from the initial absorbance change recorded in the flash photolysis kinetic traces. It decreases with [Cyt *c*], in a way similar to that previously found in fluorescence experiments (see Fig. 5), and it can be described by the expression [28]:

$$\phi_T = \frac{\phi_T^{AlPcS_4} + \phi_T^{complex} K_b[\text{Cyt } c]}{1 + K_b[\text{Cyt } c]} \quad (1)$$

This equation can be used without taking into account the diffusion quenching of the singlet excited state because on the nanosecond timescale (when intersystem crossing occurs) such quenching is negligible [28]. Hence, the complex formation affects strongly the production of $AlPcS_4$ triplets, which from extrapolation seems to indicate a ϕ_T for the complex equal to 0.09. Previously it was found that the fluorescence quantum yield of the same complex is equal to 0.065. Under a simple

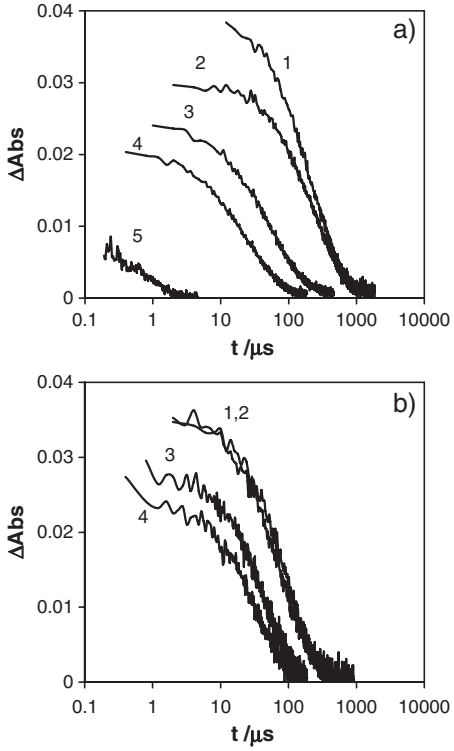

Fig. 4. Laser Flash Photolysis decays of $AlPcS_4$ in aqueous and phosphate buffer solutions. a) Curves were obtained in aqueous solution ([Cyt *c*]=0 μM (1), 0.9 μM (2), 2.3 μM (3), 5 μM (4) and 60 μM (5)) and b) curves in buffer solutions (ionic strength equal to 170 mM, [Cyt *c*]=0 μM (1), 8 μM (2), 32 μM (3), 64 μM (4)). Excitation wavelength was 570 nm and absorption wavelength 500 nm. [$AlPcS_4$]=10 μM.

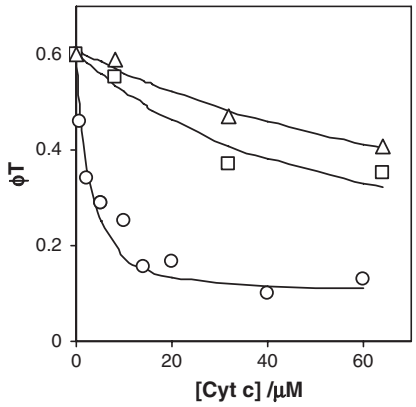

Fig. 5. Triplet quantum yields of $AlPcS_4$ in aqueous solutions (○) and buffer solutions (ionic strength equal to 17 mM (□) and 170 mM (△)).

kinetic scheme, within the complex between $AlPcS_4$ and Cyt *c*, both quantum yields can be described by the following equations:

$$\phi_f^{complex} = \frac{k_f}{k_f + k_{isc} + k_{ET}^{complex}} \quad (2)$$

$$\phi_T^{complex} = \frac{k_{isc}}{k_f + k_{isc} + k_{ET}^{complex}} \quad (3)$$

where k_f is the radiative rate constant, k_{isc} is the intersystem crossing rate constant and $k_{ET}^{complex}$ is the electron-transfer rate constant from the singlet excited state $AlPcS_4$ to Cyt *c*. With approximate values of k_f and k_{isc} known from measurements without the presence of Cyt *c*, similar values of $k_{ET}^{complex}$ are obtained if we calculate the rate constant from either $\phi_f^{complex}$ [28] or $\phi_T^{complex}$. The value obtained is around 1×10^9 s^{-1}, which is in close agreement with the result obtained from time-resolved fluorescence measurements [28]. From these measurements, K_b in buffer solutions was also measured and a good agreement with previous fluorescence measurements was reached [28]. It decreases sharply when salt is added, reaching a plateau afterwards. This ionic strength effect leads to the dissociation of the complex, which leads to the observed increase of the triplet quantum yields (Table 1).

The $AlPcS_4$ triplet lifetimes depend on [Cyt *c*] and on the ionic strength. Any interpretation of these data must be aware of the mono-exponential decays observed experimentally. The lack of detection of other components indicates that the radicals cannot be seen in these experimental constraints. Still the complex should be observed if the electron-transfer rate constant k_{ET} from $^3AlPcS_4$ to Cyt *c* was low enough. The fact

Table 1
$AlPcS_4$/Cyt *c* binding constants for different ionic strengths

Ionic strength (μ)/mM	$K_b\times10^{-3}/M^{-1}$
0.3	320
17	19
170	10

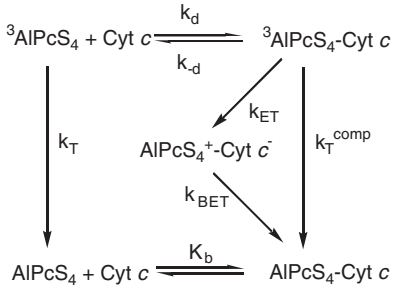

Scheme 1.

that such species are undetectable shows that they should also be short lived, with a lifetime below the detection limit of this experimental setup. Therefore both k_{ET} and k_{BET} are high (above 10^7 s^{-1}), and a standard quenching of $^3AlPcS_4$ by Cyt c is observed.

Under these assumptions, the Stern–Volmer equation should describe the experimental results [44]:

$$\frac{1}{\tau} = \frac{1}{\tau_0} + k_q[\text{Cyt } c] \tag{4}$$

where the quenching rate constant k_q is approximately given by:

$$k_q = \frac{k_T^{comp} + k_{ET}}{k_{diss} + k_T^{comp} + k_{ET}} k_{diff} \tag{5}$$

if Scheme 1 applies.

If $k_{ET} \gg k_{diss}$, k_T^{comp}, then we obtain $k_q = k_{diff}$, the so-called diffusion controlled quenching reaction limit. Otherwise, if $k_{diss} \gg k_{ET}$, k_T^{comp}, Eq. (5) becomes:

$$k_q = \frac{k_{diff}}{k_{diss}} k_{ET} = K_b k_{ET} \tag{6}$$

The complex formation in the ground state is playing an important role, when [Cyt c] is smaller than [$AlPcS_4$], and therefore much of the Cyt c is already complexed with $AlPcS_4$. Thus not all the Cyt c is available to interact with $^3AlPcS_4$, and only the protein without the dye should be taken into account, because there is no large excess of the protein. The simplicity of Eq. (1) is a consequence of considering a large excess of Cyt c. However the Cyt c native form (Cyt c_N, which is not complexed with $AlPcS_4$) concentration is lower than the Cyt c analytical concentration. The equation that enables the calculation of [Cyt c_N] is given by:

$$[\text{Cyt } c_N] = \frac{K_b[\text{Cyt } c] - 1}{2K_b} + \frac{\sqrt{K_b^2([AlPcS_4] - [\text{Cyt } c])^2 + 2K_b([AlPcS_4] + [\text{Cyt } c]) + 1}}{2K_b} \tag{7}$$

The concentration of free phthalocyanine ($AlPcS_4^{free}$) and complex (Pc–Cyt c) can then be easily calculated:

$$\left[AlPcS_4^{free}\right] = \frac{[AlPcS_4]}{1 + K_b[\text{Cyt } c_N]} \tag{8}$$

$$[\text{Pc} - \text{Cyt } c] = K_b\left[AlPcS_4^{free}\right][\text{Cyt } c_N] \tag{9}$$

because K_b is already known from previous measurements. If $1/\tau$ is plotted vs. [Cyt c_N], a linear relationship is obtained (see Fig. 6). Experimental values of k_q are then obtained for the three different buffer concentrations (see Table 2).

Table 2
Results from the Stern–Volmer analysis

Ionic strength (μ)/mM	$\tau_0/10^{-6}$ s	$k_q^{exp}/10^9$ M^{-1} s^{-1}	$k_{diff}^{calc}/10^9$ M^{-1} s^{-1}
0.3	295	17.6	44
17	100	2.1	16.3
170	94	0.3	9.0

The value obtained for k_q is large, but not as large as that observed for the quenching of the $AlPcS_4$ singlet excited state (which is 240×10^9 M^{-1} s^{-1}) [28]. These large values are above the hard-spheres diffusion limit [44] (around 8×10^9 M^{-1} s^{-1}) and can be explained by a non-homogeneous distribution of the solutes around the protein, due to the strong electrostatic interactions that are established between them. This is a rather complex phenomenon that cannot be easily addressed without several assumptions. So the electron-transfer rate constant should not be obtained by Eq. (6) without addressing this effect carefully. Rather than that, a direct measurement of the electron-transfer rate constant should be obtained in order to fully understand the behaviour observed in this system.

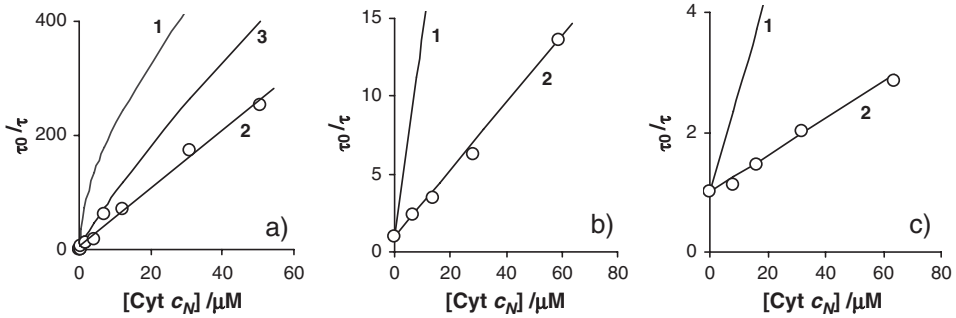

Fig. 6. Stern–Volmer plots. Straight lines represent the calculations obtained from the different models used. Curves 1 were obtained with diffusional model assuming Scheme 1 mechanism ($r_{Cyt\ c}$ = 13 Å). Curves 2 were obtained with the model derived from Scheme 2. Curve 3 is the same as curve 2, but assuming $k_- \gg k_{ET}$. a) Aqueous solution, b) buffer solution, ionic strength equal to 17 mM, and c) buffer solution, ionic strength equal to 170 mM.

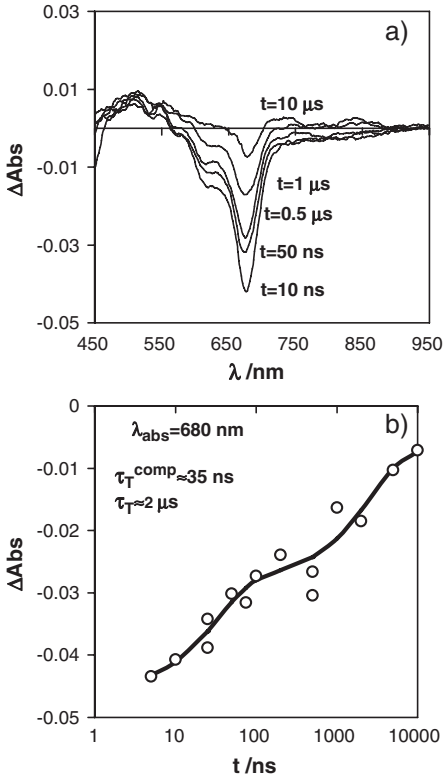

Fig. 7. a) $AlPcS_4$ transient absorption spectra at different time delays in aqueous solution ([$AlPcS_4$] = 15 μM, [Cyt *c*] = 100 μM). b) Kinetic data at λ_{abs} = 680 nm, fitted with a double exponential.

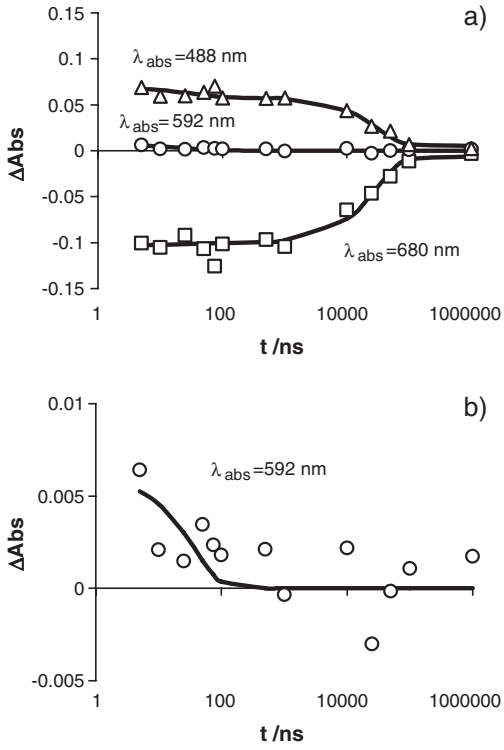

Fig. 9. a) $^3AlPcS_4$ decay kinetics at different absorption wavelengths on buffer solution ([$AlPcS_4$] = 15 μM, [Cyt *c*] = 100 μM). b) Same as a), but with the data for λ_{abs} = 592 nm amplified. Fits were done with biexponential functions.

The *Laser Flash Photolysis* equipment used has a limitation to bear in mind: it does not allow to probe events that occur below the 500 ns timescale. Any species existing at times shorter than that would not be observed and so the mono-exponential decays may be misleading. Thus Transient Absorption measurements were performed in order to get evidence of the existence of triplet excited state $AlPcS_4$ complexed with Cyt *c*. Also the appearance of $AlPcS_4$ radicals could be detected because the equipment used is sensitive to wavelengths around 800 nm.

3.3. Transient absorption spectroscopy

At [$AlPcS_4$] = 15 μM, the transient spectra have the shape expected from previous measurements on the *Laser Flash Photolysis* equipment. The triplet transient absorption spectra peak at 500 nm and a strong bleaching is observed at 680 nm. The decay of the spectra is single-exponential with a lifetime of 250 μs, in accordance with the results obtained in the Laser Flash Photolysis experiments. When a large excess of Cyt *c* is added (100 μM) a strong quenching is evident (Fig. 7). The

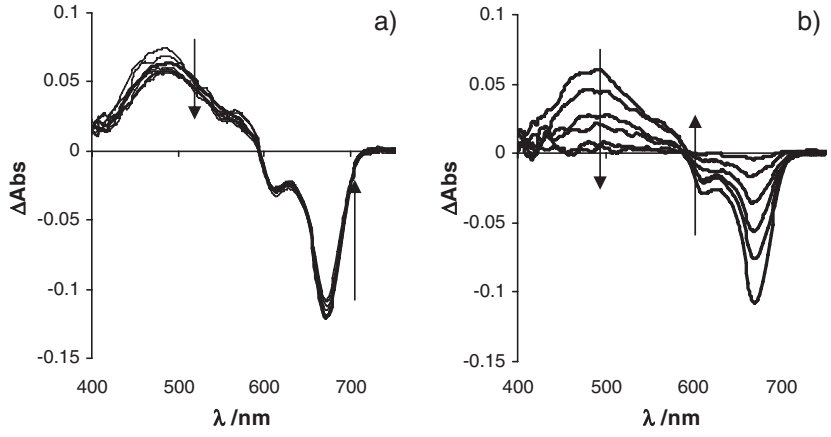

Fig. 8. $AlPcS_4$ transient absorption spectra at different time delays on buffer solution ([$AlPcS_4$] = 15 μM, [Cyt *c*] = 100 μM). a) Time delays 0 to 1000 ns and b) from 10 μs to 1 ms.

triplet formation is greatly reduced and the triplet decay kinetics is much faster. A second component appears on the triplet decay with a lifetime of about 30 ns, and therefore biexponential kinetics appears. This component is too short to be observed with Laser Flash Photolysis experiments.

In buffer solutions (ionic strength equal to 170 mM) the signal obtained is 3 times stronger, because of the ϕ_T increase (see Fig. 5). The transient spectra of the shorter component get swamped by this increase, and therefore the complex is not so easily observed. However two distinct isosbestic points are indeed observed depending on the timescales studied (Fig. 8).

The kinetics of the shortest component appears without the influence of the long component at the second isosbestic point (λ_{abs}=592 nm). At this wavelength, a weak transient absorption is detected at shorter time delays and a lifetime for the triplet state complex may be obtained by fitting (about 30 ns, see Fig. 9). This is very similar to the result obtained in aqueous solution (see Fig. 7).

4. Discussion

4.1. Cytochrome c stability in the presence of $AlPcS_4$

Cyt *c* conformation remains almost the same at $AlPcS_4$ concentrations which give a ratio [$AlPcS_4$]/[Cyt *c*] below 2. The CD spectra at the *heme* group absorption band and at the UV region do not display any significant difference as $AlPcS_4$ is added into the solution. Therefore the axial bonds between the iron and the histidine and the methionine residues are not broken. This means that the Cyt *c* redox potential remains unchanged and therefore for the range of concentrations studied on the $AlPcS_4$ triplet quenching experiments (in which Cyt *c* is in excess) the protein is in the native state.

The kinetics reveals the presence of several conformational states when Cyt *c* interacts with $AlPcS_4$. A complete description of the system requires more than one conformational substrate, and therefore those intermediates are only partially unfolded. Such long kinetics implies a complex mechanism, in which not only the diffusion of dye molecules towards the solute is required, but also it must allow time enough in order to have a rearrangement of the protein that involves the breaking of many hydrogen bonds and electrostatic interactions. For the lower $AlPcS_4$ concentration (2.26×10^{-5} M), the kinetics appears to be single-exponential, with a rate constant equal to about 6.6×10^{-4} s^{-1}. When the concentration increases to 4.4×10^{-5} M, the rate of this process remains around 8.5×10^{-4} s^{-1}, but the kinetics is no longer single-exponential and a faster component with a rate constant faster than 0.04 s^{-1} appears. Therefore by changing the $AlPcS_4$ by a factor of 2 not only more non-native species appear, but also a much faster component appears.

A complete unfolded state is, however, not reached, not only because the UV C.D. spectrum still shows the presence of α helixes, but also because there is a significant amount of Cyt *c* with the axial bond unchanged. It may be that a molten globule state, intermediate between the native and unfolded states [30], may appear for these concentrations.

4.2. $^3AlPcS_4$ quenching by Cyt c

4.2.1. Diffusion model

The $^3AlPcS_4$ quenching by Cyt *c* is characterized by k_q values above 10^{10} M^{-1} s^{-1}. Going into the roots to explain the increase of k_q above the diffusion limit of hard spheres, the presence of electrostatic interactions between them is incorporated in the Debye–Smoluchowski treatment, in which the diffusion rate constant is given by [45,46]:

$$k_d = \frac{2k_BTN}{3000\eta}\left(2+\frac{r_A}{r_B}+\frac{r_B}{r_A}\right)\frac{1}{a\int_a^\infty r^{-2}\exp[w(r,\mu)/k_BT]} \quad (10)$$

where k_B is the Boltzmann constant, N is the Avogrado number, η is the liquid viscosity, r_A and r_B are the radii of the reactants, $a=r_A+r_B$, r is the distance separating the two reactants and $w(r,\mu)$ is the potential between the interacting reactants which according to the Debye–Hückel theory is given by [45]:

$$w(r,\mu) = \frac{Z_AZ_Be^2}{2\varepsilon r} \times\left(\frac{\exp(\beta\sigma_A\sqrt{\mu})}{1+\beta\sigma_A\sqrt{\mu}}+\frac{\exp(\beta\sigma_B\sqrt{\mu})}{1+\beta\sigma_B\sqrt{\mu}}\right)\exp(-\beta r\sqrt{\mu}) \quad (11)$$

where

$$\beta = \left(\frac{8\pi Ne^2}{1000\varepsilon k_BT}\right)^{1/2} \quad (12)$$

Z_A and Z_B are the ionic charges of the reactants, ε is the static dielectric constant of the solvent, e is the electron charge, σ_A and σ_B are the radii of the reactant plus that of the dominant counterion in the ionic atmosphere and μ is the ionic strength. One important limit of Eq. (10) can be made. If $w(r,\mu)=0$ (no interactions between the reactants), Eq. (10) gives:

$$k_d = \frac{2k_BTN}{3000\eta}\left(2+\frac{r_A}{r_B}+\frac{r_B}{r_A}\right) \quad (13)$$

The dissociation rate constant k_{-d} can be calculated from the Eigen treatment of the diffusion separation of encounter pairs [45]:

$$k_{-d} = \frac{k_BT}{2\pi\eta}\frac{1}{a^2}\left(\frac{1}{r_A}+\frac{1}{r_B}\right)\frac{\exp[w(a,\mu)/k_BT]}{a\int_a^\infty r^{-2}\exp[w(r,\mu)/k_BT]} \quad (14)$$

Finally the binding constant K_b is given by the well-known Fuoss equation [47]:

$$K_b = \frac{k_d}{k_{-d}} = \frac{4\pi Na^3}{3000}\exp[-w(a,\mu)/k_BT] \quad (15)$$

This set of equations provides a framework on which diffusion rate constants may be calculated. However there are some severe limitations in this framework. The most important is that it relies on the assumption that we are dealing with hard spheres that interact with each other through electrostatic interactions. Although this may be a very good approximation

for small solutes, it is clearly a too rough approximation when proteins with an unsymmetrical charge distribution are present in the reaction. However the framework was tested in order to check how far is the present system from the assumptions of the model.

The calculation of k_d, k_{-d} and K_b was carried out with r_A=13 Å (Cyt *c* radius), r_B=7 Å ($AlPcS_4$ radius), ε_r=80.2 (water relative dielectric constant) and η=1.02 cP, and the dominant counterion was taken to be Cl^- (radius equal to 1.67 Å) for Cyt *c* and Na^+ (radius equal to 1.13 Å) for $AlPcS_4$. The ionic strength changes slightly within the range of [Cyt *c*] used, but it is enough to change significantly the electrostatic interactions and hence the diffusion processes. Therefore the solutions without phosphate buffer are not really with ionic strength equal to zero. The addition of relatively large amounts of salt keeps these changes negligible, and that is precisely what happens in the phosphate buffer solutions, but for the solutions without buffer it is important to take into account this variation.

4.2.2. Unimolecular electron-transfer in the $AlPcS_4$/Cyt c complex

There are two ways from which k_{ET} may be calculated. One that is widely used is, from Stern–Volmer plots, to calculate k_q and then from Eq. (6) k_{ET} is readily calculated if the equilibrium constants for the complex formation are known. This procedure relies on a very important assumption: $k_{-d} \gg k_{ET}$. Unless radical formation is detected and k_{-d} directly obtained, it is not possible to be completely certain of the k_{-d} value. If no radicals are observed (which is the present case), then there is a strong possibility that in fact $k_{-d} \ll k_{ET}$, which is exactly the opposite of the assumption needed to apply Eq. (6) to calculate k_{ET}. So one should be very careful when an attempt to obtain k_{ET} from Stern–Volmer plots is made.

The alternatives are to calculate theoretically the expected rate from Marcus theory [48] or try to obtain experimentally the rate from decay of the excited state complex. For this reason the measurements with nanosecond time-resolution, in order to detect this complex, were crucial. The results obtained with and without buffer pointed out to a triplet state complex lifetime of about 30 ns, which means a k_{ET} around 3×10^7 s^{-1}. This data along with those obtained previously found in the literature are shown on Fig. 10.

There are many literature reports of electron-transfer measurements involving Cyt *c* with several electron donors, which have been successfully analysed within the framework of Marcus theory for electron-transfer reactions. According to the theory, k_{ET} is given by Eq. (16) [48]:

$$k_{ET} = \sqrt{\frac{4\pi^3}{h^2 \lambda k_B T}} H_0^2 \exp(-\beta r) \exp\left(-\frac{(\Delta G^0 + \lambda)^2}{4\lambda k_B T}\right) \quad (16)$$

where λ is the reorganization energy, h is the Planck constant, k_B is the Boltzmann constant, T is the temperature, ΔG^0 is the reaction driving force, H_0 is the electronic coupling for close-contact distance between donor and acceptor, β is the distance decay constant of the electronic coupling and r is the encounter distance between the reactants. Langen et al. studied the

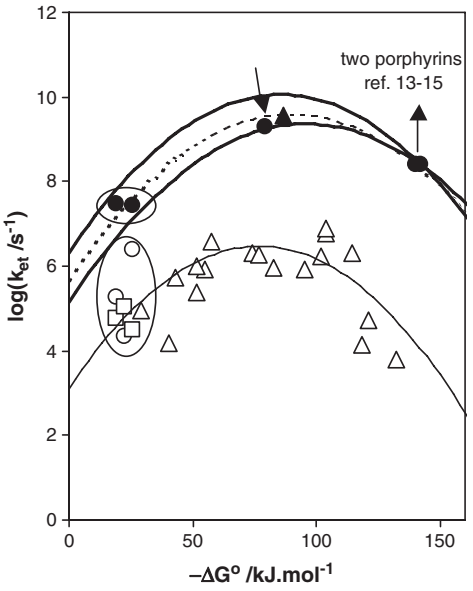

Fig. 10. Marcus plot of the electron-transfer rate constants obtained for Cyt *c* electron-transfer complexes. Dark symbols were taken from measurements of singlet excited state quenching (porphyrins [13–15] and a fullerene derivative (triangle) [27]). The arrow shows the result of the $AlPcS_4$ singlet excited state quenching [28] and in the circle are the triplet states quenching results. The open symbols are taken from Stern–Volmer analysis, using Eq. (6) [8,9]. Parabolas are fits with Marcus theory (Eq. (16)), except the bold, which were calculated from temperature dependent experiments obtained by Larsen et al. [13–15], also using Marcus theory. Dashed parabola is a fit of the dark symbols with Marcus theory, which gives reorganization energy equal to 0.93 eV.

electron-transfer between donors covalently linked to the Cyt *c* that allowed knowledge of H_0 and β across the protein [49]. The reorganization energy was also experimentally obtained, and was shown to be around 0.8 eV, where the contribution from the protein reorganization dominates the other contributions from the solvent and from the donors [50].

The reaction driving force turns out to be relatively simple to calculate, by the equation:

$$\Delta G^0 = E^0_{ox} - E^0_{red} + C \quad (17)$$

where E^0_{ox} and E^0_{red} are the redox potentials of $AlPcS_4$ triplet state and Cyt *c*, and C is the work necessary to bring together the ions:

$$C = w_p(a,\mu) - w_r(a,\mu) \quad (18)$$

where $w_p(a,\mu)$ and $w_r(a,\mu)$ are the work terms of the products and reactants respectively. So it will depend on the ionic strength as well.

The comparison with other complexes of the same type (i.e. −4 charged solutes that dock at the Cyt *c* active site) on Fig. 10 can be made because large variations of the donor-acceptor distance are not expected [28,29]. Larsen and co-workers have studied the k_{ET} temperature dependence for selected porphyrins in the singlet excited state [13–15], which ΔG^0 lies within the Marcus inverted region. They applied Marcus theory and calculated, among other values, the reorganization energy. The value they obtained was between 0.89 and 1.00 eV, and the

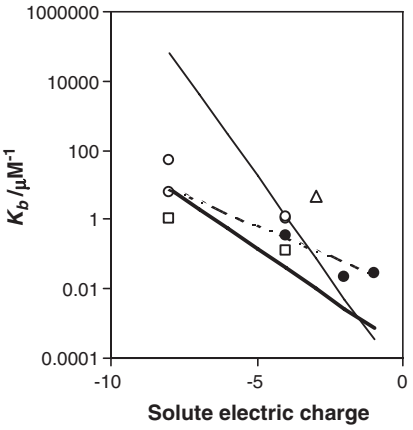

Fig. 11. Influence of the solute charge on K_b. Binding constants of water-soluble porphyrins (data taken from: Ref. [16] ○, Refs. [12,13] □ and Ref. [11] △) and sulfonated phthalocyanines (Ref. [28] ●). Dashed line is the trend of experimental results, normal line is obtained with diffusion model according to Scheme 1, bold line is obtained with diffusion model according to Scheme 2 (see text for details).

curves plotted on Fig. 10 were calculated from their data. It turns out $AlPcS_4$ excited states electron-transfer to Cyt *c* is in very good agreement with their results. In fact with the five points available it is possible to do a new fit with Eq. (16), giving a reorganization energy equal to 0.94 eV, lying on the interval range of the data by Larsen et al.

Lack of agreement is however found when a comparison is made with k_{ET} values obtained by Eq. (6). These data [8,9,50] are 3 orders of magnitude lower than our experimental values. To check out this procedure, a calculation of k_{ET} with Eq. (6) with the Stern–Volmer plots shown here on Fig. 6 was made, and a good agreement with this set of data was obtained. It would be comfortable to remain with this analysis, but it is in complete disagreement with the triplet state complex lifetime and it ignores diffusion processes that should play an important role since k_q higher than 10^{10} M^{-1} s^{-1} are observed. Also the assumption $k_{-d} \gg k_{ET}$ might be completely erroneous. Therefore it is concluded that the use of Eq. (6) gives rise to erroneous k_{ET} that underestimate it by as much as 3 orders of magnitude. If this was true, fluorescence quenching should never occur, but it does occur as it was shown previously that k_{Et} is around 10^9 s^{-1}, instead of the predicted 10^6 s^{-1} from those data.

The electronic coupling that one obtains with Fig. 10 (and that was also observed by Larsen et al.) is high, indicating that $AlPcS_4$ and the *heme* group are very close, less than 11 Å away. This also assures that the organic solute is indeed at the protein active site.

4.2.3. $AlPcS_4$/Cyt c complex formation: how does it occur?

With $k_{ET}=3\times10^7$ s^{-1} it is possible to test the diffusion model described before, where other data values, like Cyt *c* radius, were listed. This framework provides estimates of the triplet quenching that are clearly above the experimental data (Fig. 6). The numerical failure of the model could be either on the calculation of k_d or k_{-d}.

A decrease of k_d would produce this result. The framework is based on the assumption that the electric charge is homogeneously distributed on the protein surface, but it is expected that the heterogeneous charge distribution on the surface of the Cyt *c* and van der Waals interactions play an important role. Comparison with other charged synthetic receptors showed a dependence of K_b with the synthetic receptor electric charge [28], similar to the Fuoss equation. However such dependence is only acceptable if high values of *a* and $Z_{Cyt\ c}$ are introduced (14 nm and +20 respectively). For $Z_{Cyt\ c}=+8$, $Z_B=-4$ and $a=20.5$ Å, K_b is closed to the experimental values of $AlPcS_4$ and other synthetic receptors, but for $Z_B>-4$ and $Z_B<-4$ important deviations are observed (see Fig. 11). The experimental K_b for $AlPcS_1$ ($Z_B=-1$) is two orders of magnitude higher than expected, while for porphyrins with $Z_B=8$, K_b values are two orders of magnitude lower than expected from the Fuoss equation. Because K_b is not dependent on the k_{ET} value, this shows definitely that there is something wrong with the framework to calculate K_b. At a fixed Z_B there are two orders of magnitude variations of experimental values of K_b. Still the difference of slope must have an electrostatic nature in order to explain the dependence with the solute electric charge. The heterogeneous charge distribution on the protein surface is the best explanation for such effect, because it definitely changes the interaction potential given on Eq. (11). More important, previous experiments on the $AlPcS_4$ singlet excited state [28] showed that the docking site is indeed the Cyt *c* active site where the docking with other proteins is achieved. Therefore the values of k_{-d} and k_d were not calculated by an appropriate model, which should include this effect in order to explain the variation of K_b with Z_B.

Koppenol and Margoliash studied the asymmetric charge distribution on the surface of Cyt *c* [5]. It was found that only for a radius higher than 35–40 Å the electric potential field can be approximated to a spherical surface. As the solute approaches the protein at a shorter distance, the asymmetrical distribution becomes important, and Cyt *c* appears as a large dipole. So the model described is only applicable to a cavity of about 40 Å size. At shorter distances the electrostatic interaction can be either repulsive (if the molecule approaches the negative part of the dipole) or attractive (if the molecule approaches the positive region of the protein surface) in such a way that the molecules will go into the active site of the protein. The scheme for such view would be (Scheme 2).

In this scheme, $AlPcS_4$ firstly diffuses until it reaches a distance from the Cyt *c* of about 35 Å (the $AlPcS_4$...Cyt *c* encounter pair), and will rest within that cavity without

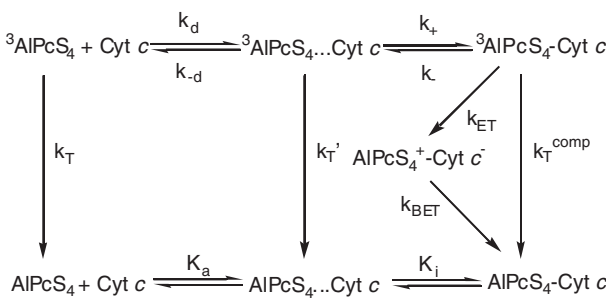

Scheme 2.

undergoing electron-transfer because it is still too far away from the *heme* group. Eventually, due to the electrostatic interaction, some molecules will meet the active site (a region with a high positive charge due to lysine residues) where they will rest long enough to undergo the electron-transfer process. Only in the active site the solute-*heme* distance is short enough in order to have an electron-transfer process in the triplet state, and therefore the K_b obtained previously is in fact:

$$K_b = K_{\text{elect}} \times K_i = \frac{[\text{AlPcS}_4\text{–Cyt } c]}{[\text{AlPcS}_4]\cdot[\text{Cyt } c]} \tag{19}$$

Calculations of K_{elect}, k_d and k_{-d} can be carried out using the model outlined previously, with $r_{\text{Cyt } c}$=35 Å. But at a shorter distance there are no analytical models of $w(r, \mu)$ available to carry out the calculations.

Fig. 11 shows how K_{elect} compares with the experimental results and with the previously calculated values of K_b. The greatest difference is that it is much smaller than the previously calculated values, and now there is a convergence for solute electric charge equal to −8. The remainder can therefore be connected with K_i. If the Scheme 2 is applicable, K_i decreases with the solute electric charge, which means that the Cyt *c* dipole can repel the solute from the proximity of the protein, possibly due to the presence of some negative charges on the protein surface. So the binding of the solute to the Cyt *c* will depend on the direction in which the solute approaches the protein. This K_i will also include other interactions of the van der Waals type, which have a much shorter range and will be important only when the solute is already almost in contact with the protein surface.

Scheme 2 can be translated in a tri-exponential decay for the triplets, which is not in accordance with experimental results. However it is possible that $k_T \approx k_T'$, or at least pretty close to, and k_{ET} may be sufficiently large to make the third exponential not observed because it is too fast to be detected. The fact that $k_{\text{ET}} \gg k_T, k_T', k_T^{\text{comp}}$ makes possible some assumptions when the kinetic scheme is resolved. The equations to take into account are:

$$-\frac{\text{d}[\text{AlPcS}_4]}{\text{d}t} = (k_d[\text{Cyt } c] + k_T)[\text{AlPcS}_4] - k_{-d}[\text{AlPcS}_4\text{...Cyt } c] \tag{20}$$

$$-\frac{\text{d}[\text{AlPcS}_4\text{...Cyt } c]}{\text{d}t} = (k_{-d} + k_+ + k_T')[\text{AlPcS}_4\text{...Cyt } c] - k_d[\text{Cyt } c][\text{AlPcS}_4] - k_-[\text{AlPcS}_4\text{–Cyt } c] \tag{21}$$

$$-\frac{\text{d}[\text{AlPcS}_4\text{–Cyt } c]}{\text{d}t} = (k_- + k_{\text{ET}} + k_T^{\text{comp}})[\text{AlPcS}_4\text{–Cyt } c] - k_+[\text{AlPcS}_4\text{...Cyt } c] \tag{22}$$

Under the steady-state approximation for AlPcS_4…Cyt *c* and AlPcS_4–Cyt *c*, an expression for the triplet lifetime may be derived. With the assumption that k_T' and k_T^{comp} are negligibly small compared with other rate constants (k_T is around 10^4 s^{-1} while k_{-d} and k_{ET} are around 10^6 s^{-1}), the following expression is obtained to fit the Stern–Volmer plots:

$$\frac{1}{\tau_T} = k_T + \frac{k_d k_{\text{ET}}}{k_{-d}\left(\frac{1}{K_i} + \frac{k_{\text{ET}}}{k_+}\right) + k_{\text{ET}}}[\text{Cyt } c] \tag{23A}$$

with:

$$K_i = \frac{k_+}{k_-} \tag{23B}$$

Eqs. (23A) and (23B) is obviously similar to Eq. (5), but can yield different results due to the more detailed description of the physical phenomena. The steady-state approximation seems also to be plausible, since the triplet decays are single-exponential under this timescale.

The biggest problem, however, is that some parameters have to be adjusted unless $k_- \gg k_{\text{ET}}$. K_i can be obtained from experimental results of K_b and the value calculated for K_{elect} through Eq. (15). Fig. 12 shows the data obtained from these experiments and calculations. It can be seen that K_i is fairly independent from the ionic strength, at least when compared with the variations of K_b (the experimental results) and of K_{elect}, which change some orders of magnitude while K_i remains between 20 and 50 M^{-1}. This parameter gives an insight as to what happens within the 40 Å shell that surrounds the protein, which is very likely much more saturated of ions than the bulk solution. So any salt concentration change within this region is smoothed by the intrinsic salt concentration in the shell even at low ionic strengths.

If $k_- \gg k_{\text{ET}}$, K_i is the only extra parameter required to calculate τ_0/τ. All other parameters are calculated as before. The solution with low ionic strength (no salt buffer added) is the one in which this approximation gets closer to the experimental results. Still it is relatively far from experiment, but it shows that the calculations give rise to data closer to experimental results if the electron-transfer rate constant is much smaller than k_-. However in the presence of salt these calculations fail completely to explain the experimental data. It seems that for

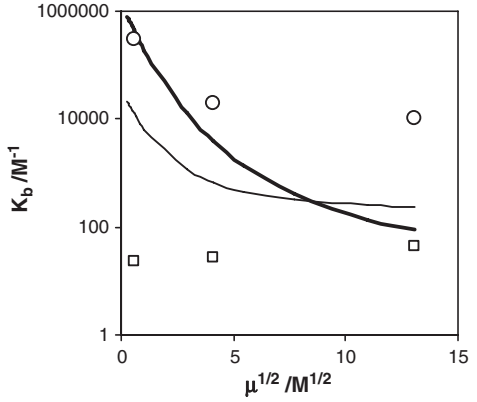

Fig. 12. Influence of the ionic strength on K_b. Bold line was calculated with a diffusion model based on Scheme 1 and normal line was based on Scheme 2. The squares are K_i values calculated through Eq. (19).

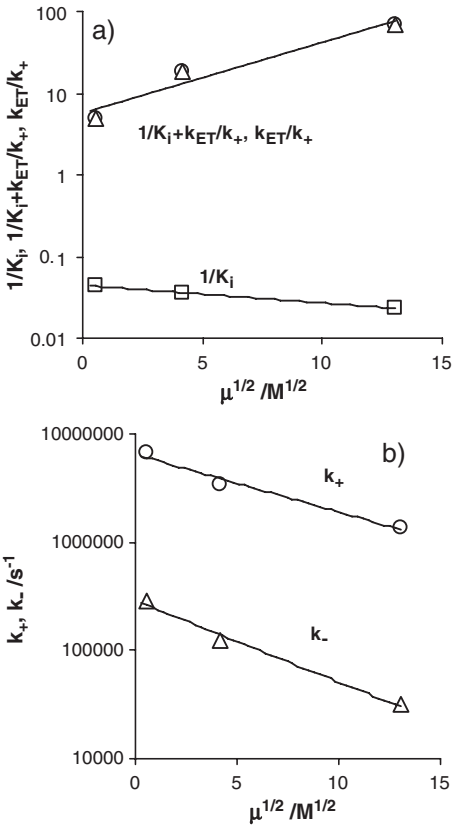

Fig. 13. Influence of the ionic strength on the calculated rate constants from Stern–Volmer plots, according to the model showed on Scheme 2.

low ionic strength k_- is small, but as the salt concentration increases the solute can exit from the active site much faster, while the electron-transfer process rate constant almost does not change. So unless there are means to estimate k_+ and k_-, this model cannot explain the experimental results without fitting k_{ET}/k_+. The fitting is straightforward, with one adjustable parameter. Fig. 13 shows the results of such fitting.

Both k_+ and k_- are within the μs and ms timescale, and change in similar way with the increase of the ionic strength. The equilibria prior electron-transfer are, therefore, rather slow, which could be an indication that the steady-state approximation is not satisfactory. On the other hand, Scheme 1 is just an approximation to get rid of an explicit non-spherical electrostatic potential of the Cyt *c* dipole when this type of analysis is performed. So in fact there is no difference between an $AlPcS_4$ in the bulk water or close to the protein: as long as there is no electron-transfer, the triplet decay will be similar. k_+ is still to a great extent part of the diffusion process, the difference is that the Cyt *c* dipolar character only manifests when the distance is close enough (see Fig. 14). At close enough distances, a so-called "close-encounter complex" may be formed, which is different in nature from that depicted on Scheme 1. Within this framework, a "dynamic complex" is formed (see Fig. 15) [28,29], but not all the possible configurations undergo the electron-transfer reaction and therefore the reaction mechanism is gated [51,52].

Such reaction mechanism may have an impact on the electron-transfer itself, because small changes of conformation

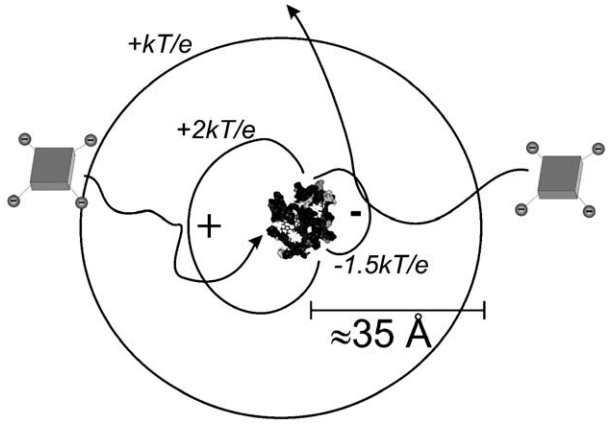

Fig. 14. Different paths a solute can undertake before a complex is formed.

can result in great changes in the electronic coupling. If these configuration changes occur on a suitable timescale, a distribution of relaxation times for the electron-transfer process appears [13,14,28,29]. This was evident on the previously published singlet-state quenching results, in which a non-exponential decay was observed. However it seems that these fluctuations occur on the nanosecond timescale ($\sim 10^9$ s^{-1}), which is a much larger rate than the 10^6 s^{-1} calculated here for k_+ and k_-. Therefore it seems that k_+ and k_- are unaffected by such phenomenon.

4.2.4. Formation of radicals

Transient-absorption spectra definitely showed that radicals are not produced, at least in significant amounts. The most plausible reason for this behaviour is the existence of a very fast back electron-transfer. Indeed the ΔG^0 for this reaction is

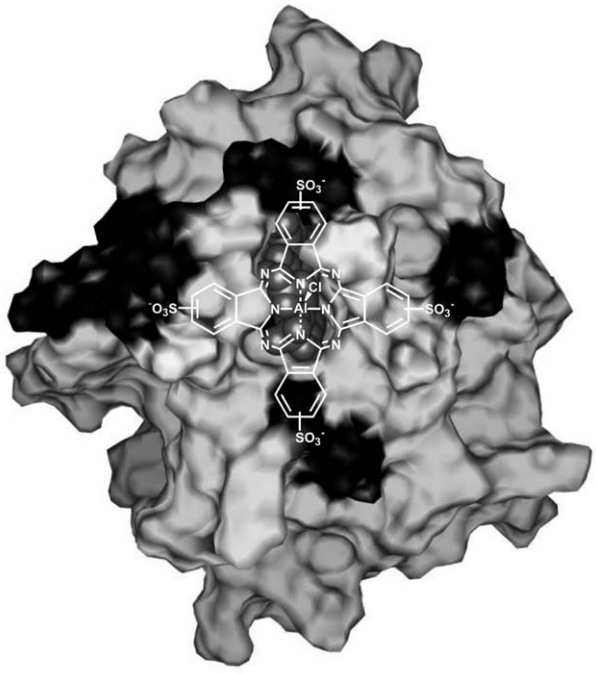

Fig. 15. Model showing Cyt *c* (with dark residues representing positively charged lysines on the protein surface) and $AlPcS_4$ at the docking site.

−0.92 eV, which, according to the Marcus theory, would yield an k_{BET} as high as 10^9 s^{-1} (see Fig. 10). The reason is that $\Delta G^0 \approx \lambda$, so it will be a process controlled mainly by the electronic coupling (hence by the distance) between donor and acceptor. This rate is far much higher than the predicted values for k_{-d}, which could be at most around 10^8 s^{-1} for higher ionic strength, but even at high buffer concentration radicals were not observed.

5. Final comments

The $^3AlPcS_4$ quenching by Cyt *c* gives rise to several interesting features, which are influenced in different ways by the medium. A $^3AlPcS_4$–Cyt *c* complex could be observed on time-resolved spectroscopic measurements, which allowed the measurement of the unimolecular electron-transfer rate constant (3×10^7 s^{-1}). Also the quenching of $^3AlPcS_4$ isolated by Cyt *c* could be studied with the Stern–Volmer equation, giving interesting insights about the mechanism of the complex formation. Heterogeneities on the charge distribution at the protein surface play an important role for the docking of the two molecules. This process is strongly influenced by the solution ionic strength, while the unimolecular electron-transfer within the complex is not influenced by such property within the experimental error. Circular Dichroism measurements, on the other hand, showed that $AlPcS_4$ can have an important impact on the Cyt *c* structure, but on 1:1 complexes the protein still remains with the native structure, hence with the same redox properties. Nevertheless, it is interesting this dual effect: for small $^3AlPcS_4$ concentrations electron-transfer might occur normally, but for higher concentrations Cyt *c* can unfold and loose its oxidative property. Finally, no radicals could be observed within the experimental conditions used. Such failure is nevertheless expected due to the large exothermic back electron-transfer reaction of this complex, which on the grounds of the Marcus theory leads us to expect an $k_{BET} \approx 10^9$. With such a competitive rate constant, the separation of the radicals does not occur and hence they cannot be observed.

Acknowledgements

This work was supported by CQE IV and the project POCTI/QUI/35398/2000. C.A.T. Laia acknowledges a post-doctoral fellowship SFRH/BPD/11567/2002. The authors thank Professor J. Costa Pessoa for the use of CD spectrometer. Dr. Isabel F. Machado is acknowledged for the assistance given on the time-resolved absorption spectroscopy measurements.

References

[1] M.W. Peczuh, A.D. Hamilton, Peptide and protein recognition by designed molecules, Chem. Rev. 100 (2000) 2479–2494.
[2] D.R. Green, J.C. Reed, Mitochondria and apoptosis, Science 281 (1998) 1309–1312.
[3] J.J. Reiners Jr., J.A. Caruso, P. Mathieu, B. Chelladurai, X.-M. Yin, D. Kessel, Release of cytochrome *c* and activation of pro-caspase-9 following lysosomal photodamage involves bid cleavage, Cell Death Differ. 9 (2002) 934–944.
[4] H. Pelletier, J. Kraut, Crystal-structure of a complex between electron-transfer partners, cytochrome-*c* peroxidase and cytochrome-*c*, Science 258 (1992) 1748–1755.
[5] W.H. Koppenol, E. Margoliash, The asymmetric distribution of charges on the surface of horse cytochrome *c* — functional implications, J. Biol. Chem. 257 (1982) 4426–4437.
[6] S. Döpner, P. Hildebrandt, F.I. Rosell, A.G. Mauk, M. von Walter, G. Buse, T. Soulimane, The structural and functional role of lysine residues in the binding domain of cytochrome *c* in the electron transfer to cytochrome *c* oxidase, Eur. J. Biochem. 261 (1999) 379–391.
[7] K.K. Clark-Ferris, J. Fisher, Topographical mimicry of the enzyme binding domain of cytochrome-*c*, J. Am. Chem. Soc. 107 (1985) 5007–5008.
[8] J.S. Zhou, E.S.V. Granada, N.B. Leontis, M.A.J. Rodgers, Photoinduced electron-transfer in self-associated complexes of several uroporphyrins and cytochrome *c*, J. Am. Chem. Soc. 112 (1990) 5074–5080.
[9] J.S. Zhou, M.A.J. Rodgers, Reactions between cytochrome-*c* and plastocyanin indicate that choice of docking sites on protein surfaces may depend on thermodynamic driving force for electron-transfer, J. Am. Chem. Soc. 113 (1991) 7728–7734.
[10] S. Speh, H. Elias, The effect of electrostatic and hydrophobic interactions on the rate of cytochrome-*c* reduction by ruthenium(ii) complexes, J. Biol. Chem. 269 (1994) 6370–6375.
[11] J. Lahiri, G.D. Fate, S.B. Ungashe, J.T. Groves, Multi-heme self-assembly in phospholipid vesicles, J. Am. Chem. Soc. 118 (1996) 2347–2358.
[12] R.W. Larsen, D.H. Omdal, R. Jasuja, S.L. Niu, D.M. Jameson, Conformational modulation of electron transfer within electrostatic porphyrin: cytochrome *c* complexes, J. Phys. Chem., B 101 (1997) 8012–8020.
[13] J.C. Croney, M.K. Helms, D.M. Jameson, R.W. Larsen, Temperature dependence of photoinduced electron transfer within self-assembled uroporphyrin–cytochrome *c* complexes, J. Phys. Chem., B 104 (2000) 973–977.
[14] J.C. Croney, M.K. Helms, D.M. Jameson, R.W. Larsen, Conformational dynamics and temperature dependence of photoinduced electron transfer within self-assembled coproporphyrin: cytochrome *c* complexes, Biophys. J. 84 (2003) 4135–4143.
[15] Q. Lin, H.S. Park, Y. Hamuro, C.S. Lee, A.D. Hamilton, Protein surface recognition by synthetic agents: design and structural requirements of a family of artificial receptors that bind to cytochrome *c*, Biopoly 47 (1998) 285–297.
[16] R.K. Jain, A.D. Hamilton, Protein surface recognition by synthetic receptors based on a tetraphenylporphyrin scaffold, Org. Lett. 2 (2000) 1721–1723.
[17] Y. Wei, G.L. McLendon, A.D. Hamilton, M.A. Case, C.B. Purring, Q. Lin, H.S. Park, C.-S. Lee, T. Yu, Disruption of protein–protein interactions: design of a synthetic receptor that blocks the binding of cytochrome *c* to cytochrome *c* peroxidase, Chem. Commun. 17 (2001) 1580–1581.
[18] R.K. Jain, A.D. Hamilton, Designing protein denaturants: synthetic agents induce cytochrome *c* unfolding at low concentrations and stoichiometries, Angew. Chem., Int. Ed. Engl. 41 (2002) 641–643.
[19] A.J. Wilson, K. Groves, R.K. Jain, H.S. Park, A.D. Hamilton, Directed denaturation: room temperature and stoichiometric unfolding of cytochrome *c* by a metalloporphyrin dimer, J. Am. Chem. Soc. 125 (2003) 4420–4421.
[20] J.T. Ernst, J. Becerril, H.S. Park, H. Yin, A.D. Hamilton, Design and application of an alpha-helix-mimetic scaffold based on an oligoamide-foldamer strategy: antagonism of the bak BH3/Bcl-xL complex, Angew. Chem., Int. Ed. Engl. 115 (2003) 553–557.
[21] T. Aya, A.D. Hamilton, Tetrabiphenylporphyrin-based receptors for protein surfaces show sub-nanomolar affinity and enhance unfolding, Bioorg. Med. Chem. Lett. 13 (2003) 2651–2654.
[22] L. Baldini, A.J. Wilson, J. Hong, A.D. Hamilton, Pattern-based detection of different proteins using an array of fluorescent protein surface receptors, J. Am. Chem. Soc. 126 (2004) 5656–5657.
[23] E. Sedlák, M. Antalík, Coulombic and noncoulombic effect of polyanions on cytochrome *c* structure, Biopoly 46 (1998) 145–154.
[24] H. Takashima, S. Shinkai, I. Hamachi, Ru(bpy)(3)-based artificial receptors toward a protein surface: selective binding and efficient photoreduction of cytochrome *c*, Chem. Commun. 23 (1999) 2345–2346.

[25] T. Oshima, M. Goto, S. Furusaki, Complex formation of cytochrome *c* with a calixarene carboxylic acid derivative: a novel solubilization method for biomolecules in organic media, Biomacromolecules 3 (2002) 438–444.
[26] J. Gong, P. Yao, H. Duan, M. Jiang, S. Gu, L. Chunyu, Structural transformation of cytochrome *c* and apo cytochrome *c* induced by sulfonated polystyrene, Biomacromolecules 4 (2003) 1293–1300.
[27] M. Braun, S. Atalick, D.M. Guldi, H. Lanig, M. Brettreich, S. Burghardt, M. Hatzimarinaki, E. Ravanelli, M. Prato, R. van Eldik, A. Hirsch, Electrostatic complexation and photoinduced electron transfer between Zn–cytochrome *c* and polyanionic fullerene dendrimers, Chem. Eur. J. 9 (2003) 3867–3875.
[28] C.A.T. Laia, S.M.B. Costa, D. Phillips, A. Beeby, Electron-transfer kinetics in sulfonated aluminum phthalocyanines/cytochrome *c* complexes, J. Phys. Chem., B 108 (2004) 7506–7514.
[29] C.A.T. Laia, S.M.B. Costa, Interactions of a sulfonated aluminum phthalocyanine and cytochrome *c* in micellar systems: binding and electron-transfer kinetics, J. Phys. Chem., B 108 (2004) 17188–17197.
[30] I. Bertini, P. Turano, P.R. Vasos, A. Bondon, S. Chevance, G. Simonneaux, Cytochrome *c* and SDS: a molten globule protein with altered axial ligation, J. Mol. Biol. 336 (2004) 489–496.
[31] J.D. Cortese, A.L. Voglino, C.R. Hackenbrock, Persistence of cytochrome-*c* binding to membranes at physiological mitochondrial intermembrane space ionic-strength, Biochim. Biophys. Acta 1228 (1995) 216–228.
[32] I.L. Nantes, M.R. Zucchi, O.R. Nascimento, A. Faljoni-Alario, Effect of heme iron valence state on the conformation of cytochrome *c* and its association with membrane interfaces — a CD and EPR investigation, J. Biol. Chem. 276 (2001) 153–158.
[33] C.J.A. Wallace, I. Clark-Lewis, Functional-role of heme ligation in cytochrome-*c* — effects of replacement of methionine-80 with natural and nonnatural residues by semisynthesis, J. Biol. Chem. 267 (1992) 3852–3861.
[34] F. Sinibaldi, L. Fiorucci, G. Mei, T. Ferri, A. Desideri, F. Ascoli, R. Santucci, Cytochrome *c* reconstituted from two peptide fragments displays native-like redox properties, Eur. J. Biochem. 268 (2001) 4537–4543.
[35] D. Phillips, Chemical mechanisms in photodynamic therapy with phthalocyanines, Prog. React. Kinet. 22 (1997) 176–300.
[36] G. Blauer, N. Sreerama, R.W. Woody, Optical-activity of hemoproteins in the soret region — circular-dichroism of the heme undecapeptide of cytochrome-*c* in aqueous-solution, Biochemistry 32 (1993) 6674–6679.
[37] P.P. Levin, S.M.B. Costa, L.F.V. Ferreira, J.M. Lopes, F.R. Ribeiro, Delayed fluorescence induced by molecular oxygen quenching of zinc tetraphenylporphyrin triplets at gas/solid interfaces of silica and zeolite, J. Phys. Chem., B 101 (1997) 1355–1363.
[38] L.F.V. Ferreira, I.F. Machado, J.P. Da Silva, A.S. Oliveira, A diffuse reflectance comparative study of benzyl inclusion within microcrystalline cellulose and beta-cyclodextrin, Photochem. Photobiol. Sci. 3 (2004) 174–181.
[39] S.M. Andrade, T.I. Carvalho, M.I. Viseu, S.M.B. Costa, Conformational changes of beta-lactoglobulin in sodium bis(2-ethylhexyl) sulfosuccinate reverse micelles — a fluorescence and CD study, Eur. J. Biochem. 271 (2004) 734–744.
[40] R. Santucci, F. Ascoli, The Soret circular dichroism spectrum as a probe for the heme Fe(III)–Met(80) axial bond in horse cytochrome *c*, J. Inorg. Biochem. 68 (1997) 211–214.
[41] G. Tsaprailis, D.W.S. Chan, A.M. English, Conformational states in denaturants of cytochrome *c* and horseradish peroxidases examined by fluorescence and circular dichroism, Biochemistry 37 (1998) 2004–2016.
[42] S. Oellerich, H. Wackerbarth, P. Hildebrandt, Spectroscopic characterization of nonnative conformational states of cytochrome *c*, J. Phys. Chem., B 106 (2002) 6566–6580.
[43] P.L. Privalov, G.I. Makhatadze, Protein interactions with urea and guanidinium chloride — a calorimetric study, J. Mol. Biol. 226 (1992) 491–505.
[44] M. Sikorski, E. Krystkowiak, R.P. Steer, The kinetics of fast fluorescence quenching processes, J. Photochem. Photobiol., A Chem. 117 (1998) 1–16.
[45] R. Ballardini, M.T. Gandolfi, V. Balzani, F. Scandola, Ionic-strength dependence of diffusion and association constants obtained from luminescence quenching experiments, Gazz. Chim. Ital. 117 (1987) 769–772.
[46] D.M. Togashi, S.M.B. Costa, Steady state and dynamic quenching of zinc tetramethylpyridylporphyrin by methyl viologen ion pairs, salt effects, New J. Chem. 26 (2002) 1774–1783.
[47] R.M. Fuoss, Ionic association. 3. The equilibrium between ion pairs and free ions, J. Am. Chem. Soc. 80 (1958) 5059–5061.
[48] R.A. Marcus, N. Sutin, Electron transfers in chemistry and biology, Biochim. Biophys. Acta 811 (1985) 265–322.
[49] R. Langen, I-Jy Chang, J.P. Germanas, J.H. Richards, J.R. Winkler, H.B. Gray, Electron-tunneling in proteins — coupling through a beta-strand, Science 268 (1995) 1733–1735.
[50] D.E. Khoshtariya, J. Wei, H. Liu, H. Yue, D.H. Waldeck, Charge-transfer mechanism for cytochrome *c* adsorbed on nanometer thick films. Distinguishing frictional control from conformational gating, J. Am. Chem. Soc. 125 (2003) 7704–7714.
[51] B.M. Hoffman, M.A. Ratner, Gated electron-transfer — when are observed rates controlled by conformational interconversion, J. Am. Chem. Soc. 109 (1987) 6237–6243.
[52] B.M. Hoffman, L.M. Celis, D.A. Cull, A.D. Patel, J.L. Seifert, K.E. Wheeler, J. Wang, J. Yao, I.V. Kurnikov, J.M. Nocek, Differential influence of dynamic processes on forward and reverse electron transfer across a protein–protein interface, Proc. Natl. Acad. Sci. 102 (2005) 3564–3569.